The Astronomical Journal, 141:8 (7pp), 2011 January doi:10.1088/0004-6256/141/1/8

WASP-37b: A 1.8 M_J EXOPLANET TRANSITING A METAL-POOR STAR

E. K. Simpson[1], F. Faedi[1], S. C. C. Barros[1], D. J. A. Brown[2], A. Collier Cameron[2], L. Hebb[3], D. Pollacco[1], B. Smalley[4], I. Todd[1], O. W. Butters[5], G. Hébrard[6], J. McCormac[1], G. R. M. Miller[2], A. Santerne[7], R. A. Street[8], I. Skillen[9], A. H. M. J. Triaud[10], D. R. Anderson[4], J. Bento[11], I. Boisse[6], F. Bouchy[6,12], B. Enoch[2], C. A. Haswell[13], C. Hellier[4], S. Holmes[13], K. Horne[2], F. P. Keenan[1], T. A. Lister[8], P. F. L. Maxted[4], V. Moulds[1], C. Moutou[7], A. J. Norton[13], N. Parley[2], F. Pepe[10], D. Queloz[10], D. Segransan[10], A. M. S. Smith[4], H. C. Stempels[14], S. Udry[10], C. A. Watson[1], R. G. West[5], and P. J. Wheatley[11]

[1] Astrophysics Research Centre, School of Mathematics and Physics, Queen's University, Belfast BT7 1NN, UK
[2] School of Physics and Astronomy, University of St Andrews, North Haugh, St Andrews, Fife KY16 9SS, UK
[3] Department of Physics and Astronomy, Vanderbilt University, Nashville, TN 37235, USA
[4] Astrophysics Group, Keele University, Staffordshire ST5 5BG, UK
[5] Department of Physics and Astronomy, University of Leicester, Leicester LE1 7RH, UK
[6] Institut d'Astrophysique de Paris, UMR7095 CNRS, Université Pierre & Marie Curie, F-75014 Paris, France
[7] Laboratoire d'Astrophysique de Marseille, 38 rue Frédéric Joliot-Curie, F-13388 Marseille cedex 13, France
[8] Las Cumbres Observatory Global Telescope Network, 6740 Cortona Drive Suite 102, Goleta, CA 93117, USA
[9] Isaac Newton Group of Telescopes, Apartado de Correos 321, E-38700 Santa Cruz de la Palma, Tenerife, Spain
[10] Observatoire de Genève, Université de Genève, 51 Ch. des Maillettes, CH-1290 Sauverny, Switzerland
[11] Department of Physics, University of Warwick, Coventry CV4 7AL, UK
[12] Observatoire de Haute-Provence, CNRS/OAMP, F-04870 St Michel l'Observatoire, France
[13] Department of Physics and Astronomy, The Open University, Milton Keynes MK7 6AA, UK
[14] Department of Physics and Astronomy, Uppsala University, Box 516, SE-751 20 Uppsala, Sweden
Received 2010 August 17; accepted 2010 September 30; published 2010 December 7

ABSTRACT

We report on the discovery of WASP-37b, a transiting hot Jupiter orbiting an $m_v = 12.7$ G2-type dwarf, with a period of 3.577469 ± 0.000011 d, transit epoch $T_0 = 2455338.6188 \pm 0.0006$ (HJD; dates throughout the paper are given in Coordinated Universal Time (UTC)), and a transit duration $0.1304^{+0.0018}_{-0.0017}$ d. The planetary companion has a mass $M_p = 1.80 \pm 0.17\ M_J$ and radius $R_p = 1.16^{+0.07}_{-0.06}\ R_J$, yielding a mean density of $1.15^{+0.12}_{-0.15}\ \rho_J$. From a spectral analysis, we find that the host star has $M_\star = 0.925 \pm 0.120\ M_\odot$, $R_\star = 1.003 \pm 0.053\ R_\odot$, $T_{\rm eff} = 5800 \pm 150$ K, and $[{\rm Fe/H}] = -0.40 \pm 0.12$. WASP-37 is therefore one of the lowest metallicity stars to host a transiting planet.

Key words: planetary systems – stars: individual (WASP-37, GSC 00326-00658) – techniques: photometric – techniques: spectroscopic

1. INTRODUCTION

Extrasolar planets show a huge diversity in their properties and this has important implications for theories of planet formation, structure, and evolution. Systems with high orbital inclinations, in which the planet transits across the face of the host star as seen from Earth, are extremely valuable as they allow us to precisely measure many fundamental planetary properties, including radius, mass, and density, which can be used to test these theories (Haswell 2010).

The parameter space which we are able to explore with transiting planets is biased by instrumental and observational limitations. However, many challenges faced by the current surveys are being overcome by the ability to decrease systematic noise and optimize follow-up strategies. Although the majority of the ~100 transiting planets thus far discovered are short-period, Jupiter-sized objects, they show a remarkable variety in their physical and dynamical characteristics, such as the extreme eccentricity of HD 80606b (Naef et al. 2001; Laughlin et al. 2009; Moutou et al. 2009; Fossey et al. 2009; Garcia-Melendo & McCullough 2009), the ultra-short period of WASP-19b (Hebb et al. 2010), and the puzzlingly low densities of WASP-17b (Anderson et al. 2010) and Kepler-7b (Latham et al. 2010).

Here we describe the properties of a new transiting planet discovered by the SuperWASP survey, WASP-37b. SuperWASP has been a major contributor to the discovery of bright ($9 < m_v < 13$) transiting planets since it began operation in 2004 (Pollacco et al. 2006). The project runs two stations, SuperWASP on La Palma, Canary Islands, and WASP-S at SAAO in South Africa, each with a field of view of almost 500 deg^2. A number of recent upgrades have been implemented to reduce systematic noise and improve photometric precision. These include reducing temperature fluctuations, which cause changes in the camera focus, by installing heating tubes, air conditioning, and improving dome insulation. As a consequence, the variation in the stellar FWHM during the course of a night has been halved. For more details, see Barros (2010).

The planet host star WASP-37 resides in an equatorial region of the sky which is monitored by both WASP instruments, significantly increasing the amount of data collected on the target. It is accessible to observatories in both hemispheres and we present follow-up photometric and spectroscopic observations taken to establish the planetary nature of the transiting object and characterize it using the RISE (Liverpool Telescope), Spectral (Faulkes Telescope South), SOPHIE (1.93 m OHP), and CORALIE (Swiss 1.2 m) instruments.

This paper is structured as follows: Section 2 describes the observations, including the discovery data and photometric and spectroscopic follow-up. The results of the derived system parameters are presented in Section 3, including the stellar and planetary properties. Finally, we discuss our findings in Section 4.

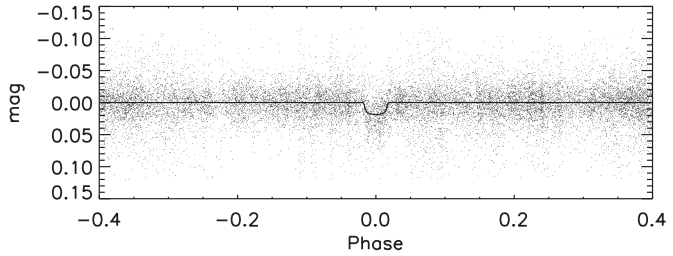

Figure 1. Combined, unbinned SuperWASP light curve for WASP-37, folded on the orbital period of $P = 3.577$ d. Superimposed is the model transit light curve, based on the system parameters determined from a global fit; see Section 3.2.

2. OBSERVATIONS

2.1. SuperWASP Photometry

WASP-37 is a $V = 12.7$ mag star in the constellation Virgo, located at $\alpha_{J2000} = 14^{h}47^{m}46^{s}.57$, $\delta_{J2000} = +01^{\circ}03'53''.9$ (GSC 00326-00658; 2MASS 14474655+0103538). It was observed by SuperWASP (La Palma) between March and June in 2008 and 2009, and by WASP-S (South Africa) during 2008 June to July and 2009 March to July. A total of 22,593 photometric data points were obtained during these intervals. The pipeline-processed data were de-trended and searched for transits using the methods described in Cameron et al. (2006). A periodic, transit-like signature was detected independently at the same period (3.58 d) in multiple cameras and in successive seasons, strongly suggesting that the transits were real, despite the faint magnitude. The folded light curve is shown in Figure 1 with the best-fit model.

The star underwent several consistency tests aimed at eliminating false positives. It is isolated within the WASP photometric aperture in the Digitized Sky Survey (DSS) image, ruling out resolved blends. We also checked for signatures of unresolved blends (see Cameron et al. 2007): no significant ellipsoidal variability was measurable in the WASP light curve folded on the transit period, nor any signs of a secondary eclipse. Moreover, the transit depth and duration yielded a planet-like radius for the companion, and a stellar density appropriate to a main-sequence host star of the effective temperature derived from the 2MASS colors. Having passed all these tests, the star was selected for follow-up observations.

2.2. Photometric Follow-up

We obtained two further transit light curves of WASP-37 in order to refine the photometric parameters, and they are shown in Figure 2. All photometric data presented in this paper are available from the NStED database.[15]

A partial transit was observed with LT/RISE on 2010 May 21. The full transit was not obtainable as the star set below the observing limits of the LT prior to egress. RISE is a frame transfer CCD located on the robotic 2.0 m Liverpool Telescope (LT) on La Palma with a broadband $V + R$ filter (Steele et al. 2008; Gibson et al. 2008). The telescope was defocused by -1.0 mm to give FWHM = 17 pixels = 9.2 arcsec, and the CCD was used in 2×2 binning mode with an exposure time of 65 s and effectively no dead time. This allowed 215 images to be taken over the 3.9 hr period, including 1 hr of observations before transit. The data were reduced using the ULTRACAM pipeline (Dhillon et al. 2007) and differential photometry was performed relative to five nearby bright stars using an 18 pixel radius aperture.

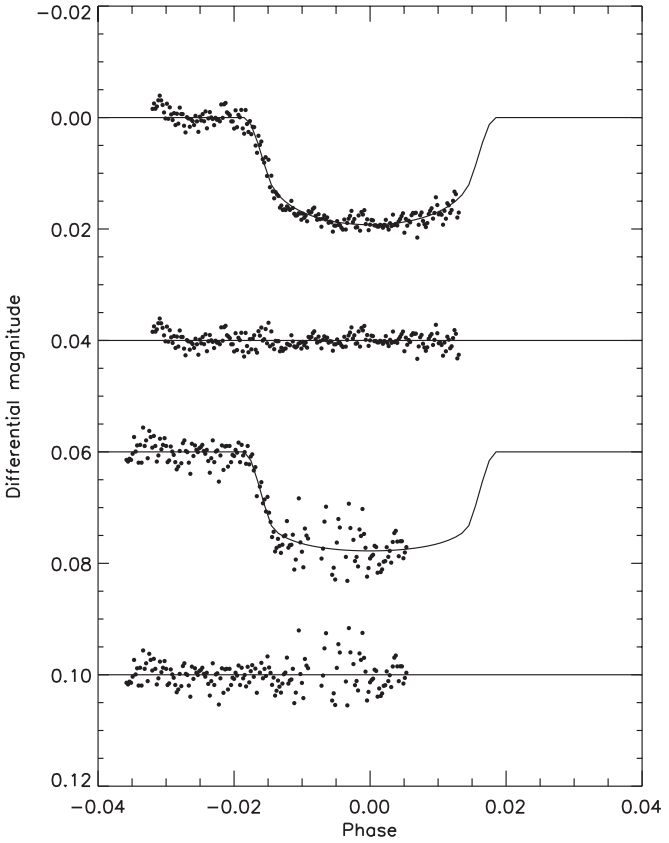

Figure 2. Photometry of transit events of WASP-37b on 2010 May 21 and June 30. The light curves have been offset from zero by arbitrary amounts for clarity. Superimposed are the model transit light curves based on the determined system parameters; see Section 3.2. Residuals from the fit are displayed underneath.

A further partial transit was obtained on 2010 June 30 with the Spectral[16] camera (FS01) on the LCOGT 2.0 m Faulkes Telescope South (FTS, Siding Spring, Australia). The Pan-STARRS-Z filter was used with the instrument in binning 2×2 mode, giving 0.303 arcsec/pixel, and no defocusing. The exposure time was 45 s, and 169 images were taken in the 3.5 hr period. Data were reduced using a pipeline[17] written at the Liverpool John Moores University, then differential photometry performed using the IRAF/DAOPHOT[18] package. Eight comparison stars were used with an 8 pixel radius aperture. Points with error bars larger than 0.01 mag were removed from the second half of the data set. These were likely caused by passing cloud, and the observation was stopped prematurely due to bad weather.

2.3. Spectroscopic Follow-up

In order to establish the planetary nature and determine the stellar parameters, we obtained follow-up spectroscopic observations. Five spectra were taken between 2010 April 17 and May 28 with the stabilized echelle spectrograph SOPHIE at the 1.93 m telescope of Observatoire de Haute-Provence (Perruchot et al. 2008; Bouchy et al. 2009). The observations

[15] http://nsted.ipac.caltech.edu.

[16] http://lcogt.net/en/network/2m.

[17] http://telescope.livjm.ac.uk/Info/TelInst/Pipelines.

[18] IRAF is distributed by the National Optical Astronomy Observatory, which is operated by the Association of Universities for Research in Astronomy, Inc., under cooperative agreement with the National Science Foundation.

Table 1
Radial Velocity (RV) and Line Bisector Span (V_{span}) Measurements of WASP-37

BJD (2,400,000+)	RV (km s^{-1})	σ_{RV} (km s^{-1})	V_{span} (km s^{-1})	Instrument
55304.4975	7.892	0.012	0.024	SOPHIE
55305.4660	8.223	0.014	−0.028	SOPHIE
55334.5449	8.196	0.019	0.004	SOPHIE
55336.4764	7.825	0.021	−0.088	SOPHIE
55345.4618	8.115	0.018	0.013	SOPHIE
55305.7532	8.152	0.018	−0.024	CORALIE
55310.8236	7.678	0.043	−0.029	CORALIE
55311.8514	7.919	0.025	−0.033	CORALIE
55312.8266	8.064	0.031	−0.091	CORALIE
55321.7716	7.668	0.023	0.058	CORALIE
55324.7114	7.769	0.022	−0.011	CORALIE
55325.6868	7.776	0.024	−0.025	CORALIE
55376.6684	8.103	0.031	−0.004	CORALIE

were all made with a signal-to-noise ratio (S/N) of ∼20 in order to minimize the charge transfer inefficiency (CTI) effect (Bouchy et al. 2009). Two 3 arcsec diameter optical fibers were used: the first centered on the target and the second on the sky to simultaneously measure the background to remove contamination from scattered moonlight. A further eight spectra were obtained with the CORALIE Fiber-Fed Echelle Spectrograph on the Swiss 1.2 m telescope at ESO-La Silla, Chile, between 2010 April 19 and June 29 with S/N ∼ 10–20 in dark/gray time to minimize contamination from scattered moonlight. The data were processed using the standard pipeline (Baranne et al. 1996; Pepe et al. 2002).

The radial velocities (RVs) and line bisector spans (V_{span}; see Toner & Gray 1988) derived from cross correlation are shown in Table 1 and plotted with the best-fit model in Figure 3. No significant correlation is seen between the bisector span and RV, which supports the signal's origin as a planetary companion rather than a blended eclipsing binary system (Queloz et al. 2001). A Spearman rank–order correlation test also indicates that any correlation between the RVs and bisector is weak, with a probability of correlation of 0.12.

3. RESULTS

3.1. Stellar Parameters

We used several techniques to infer the fundamental stellar properties of WASP-37 and the results are shown in Table 2. We first performed a spectral analysis using the methods given in Gillon et al. (2009). The individual CORALIE and SOPHIE spectra from the standard reduction pipeline were co-added to produce a single spectrum with an average S/N of around 60:1. The Hα line was used to determine the effective temperature (T_{eff}), while the Na I D and Mg I b lines were used as surface gravity ($\log g$) diagnostics. This yielded the values $T_{eff} = 5800 \pm 150$ K and $\log g = 4.25 \pm 0.15$. The effective temperature indicates that the star is of spectral type G2 (Gray 2008).

The value for microturbulence (v_{mic}) was determined from Fe I using the Magain (1984) method. We assumed a value for macroturbulence (v_{mac}) of 3.6 ± 0.3 km s^{-1} based on the tabulation by Gray (2008), and an instrumental FWHM of 0.11 ± 0.01 Å, determined from the telluric lines around 6300 Å. The projected stellar rotation velocity ($v \sin i$) was determined by fitting the profiles of several unblended Fe I lines, giving a best-fitting value of $v \sin i = 2.4 \pm 1.6$ km s^{-1}.

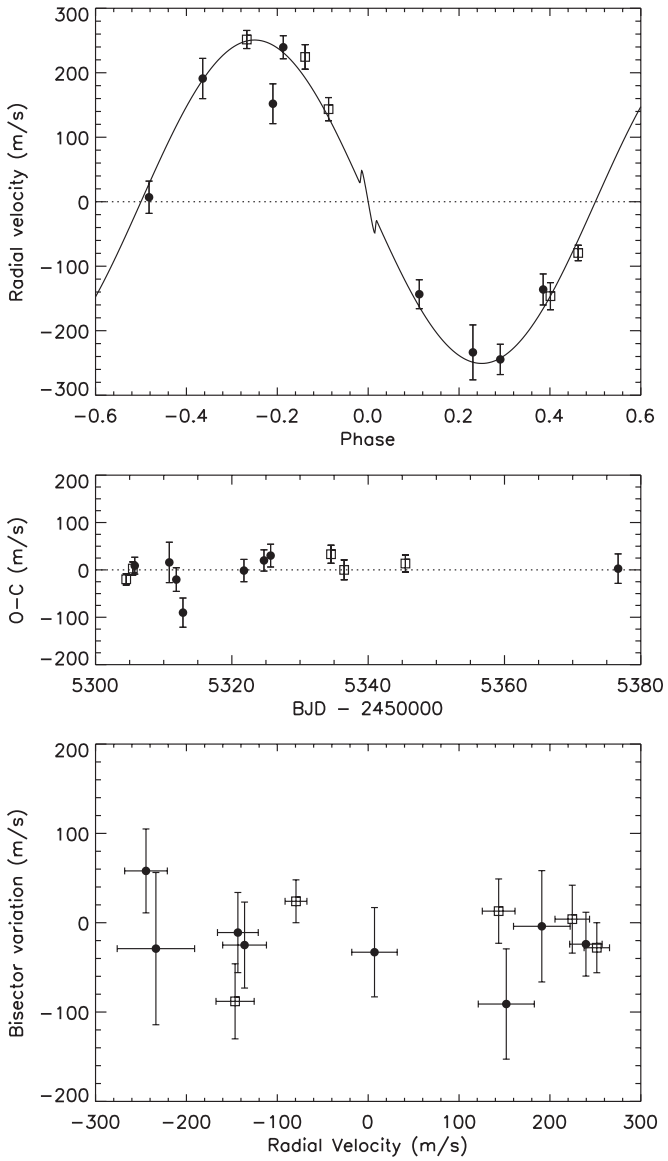

Figure 3. Upper panel: phase folded RV measurements of WASP-37, combining data from the Swiss 1.2 m/CORALIE (filled circles) and OHP/SOPHIE (open squares), and superimposed with the best-fit model RV curve based on the determined system parameters; see Section 3.2. The center-of-mass velocities, $\gamma_{SOPHIE} = 7.9714$ km s^{-1} and $\gamma_{CORALIE} = 7.9116$ km s^{-1}, were subtracted from the RVs. The predicted RM effect is shown for a spin orbit aligned system with $v \sin i = 2.4 \pm 1.6$ km s^{-1}. Middle panel: residuals from the orbital fit plotted against time. No long-term trend is visible. Lower panel: the bisector span measurements as a function of RV, showing no correlation. The uncertainties in the bisectors were taken as twice the RV uncertainties.

Elemental abundances were determined from equivalent-width measurements of several clean and unblended lines. The quoted errors include the uncertainties in T_{eff}, $\log g$, and v_{mic}, as well as the scatter due to measurement and atomic data uncertainties. We obtain [Fe/H] $= -0.4 \pm 0.12$ and $\log A(\mathrm{Li}) = 2.23 \pm 0.13$. Interstellar Na D lines are present in the spectra with equivalent widths of ∼100–150 mÅ, indicating an extinction of $E(B - V) = 0.05$ using the calibrations of Munari & Zwitter (1997).

Transit light curves provide a measure of the mean stellar density ($\rho_\star$) which can be used as a luminosity indicator for stellar evolutionary models (Sozzetti et al. 2007). We used a Markov Chain Monte Carlo (MCMC) approach to globally

Table 2
Stellar Parameters of WASP-37

Parameter (Unit)	Value
Photometric and spatial properties	
R.A. (J2000)	14:47:46.57
Decl. (J2000)	+01:03:53.9
V (mag)	12.704 ± 0.149
$B-V$ (mag)	0.600 ± 0.050
J (mag)	11.499 ± 0.022
H (mag)	11.181 ± 0.026
K_s (mag)	11.093 ± 0.023
$\mu_{R.A.}$ (mas year^{-1})	−23.2 ± 5.4
$\mu_{decl.}$ (mas year^{-1})	22.8 ± 5.4
U (km s^{-1})	−27.2 ± 3.4
V (km s^{-1})	7.8 ± 14.0
W (km s^{-1})	45.5 ± 3.4
Galactic longitude, l (deg)	355
Galactic latitude, b (deg)	52
Spectroscopic properties	
$T_{\rm eff}$ (K)	5800 ± 150
log g (cgs)	4.25 ± 0.15
$v_{\rm mic}$ (km s^{-1})	1.0 ± 0.2
$v_{\rm mac}$ (km s^{-1})	3.6 ± 0.3
$v \sin i$ (km s^{-1})	2.4 ± 1.6
[Fe/H]	−0.40 ± 0.12
[Na/H]	−0.38 ± 0.16
[Mg/H]	−0.12 ± 0.10
[Si/H]	−0.27 ± 0.08
[Ca/H]	−0.25 ± 0.13
[Sc/H]	−0.19 ± 0.16
[Ti/H]	−0.28 ± 0.14
[V/H]	−0.30 ± 0.15
[Cr/H]	−0.37 ± 0.16
[Mn/H]	−0.56 ± 0.10
[Co/H]	−0.41 ± 0.17
[Ni/H]	−0.37 ± 0.08
log A(Li)	2.23 ± 0.13
$E(B-V)$	0.05
Derived properties	
$M_\star$ ($M_\odot$)	0.925 ± 0.120
$R_\star$ ($R_\odot$)	1.003 ± 0.053
$\rho_\star$ ($\rho_\odot$)	$0.931^{+0.064}_{-0.099}$
L_* ($L_\odot$)	$0.953^{+0.184}_{-0.114}$
Age (Gyr)	11^{+3}_{-4}
Distance (pc)	343 ± 36
Spectra type	G2V

Notes. The photometric and spatial properties are taken from or derived using the following sources: V (TASS; Droege et al. 2006), $B-V$ (Casagrande et al. 2010), J, H, K_s (2MASS; Skrutskie et al. 2006), proper motions (NOMAD; Zacharias et al. 2005), space velocities (see Section 3.1.1), and galactic coordinates (NED). The spectroscopic and derived properties are determined from the spectroscopic analysis described in Section 3.1. $M_\star$ is the mean of the masses found from the empirical relationship of Torres et al. (2010) and stellar models; $\rho_\star$ is found from the light curve geometry; and the stellar radius is derived from $\rho_\star$ and $M_\star$. L_* and age are determined from stellar models.

model the photometric and RV data (see Section 3.2) and obtained $\rho_\star = 0.931^{+0.064}_{-0.099}\ \rho_\odot$. Values of $T_{\rm eff}$, [Fe/H], and $\rho_\star$ were compared with the theoretical stellar evolutionary models of Yi et al. (2001) to obtain the following stellar properties: $M_\star = 0.849^{+0.067}_{-0.040}\ M_\odot$, $R_\star = 0.977^{+0.045}_{-0.042}\ R_\odot$, $L_* = 0.953^{+0.184}_{-0.114}\ L_\odot$, $\log g_{\rm iso} = 4.39^{+0.02}_{-0.03}$, and an age of 11^{+3}_{-4} Gyr. The model isochrones are shown in Figure 4.

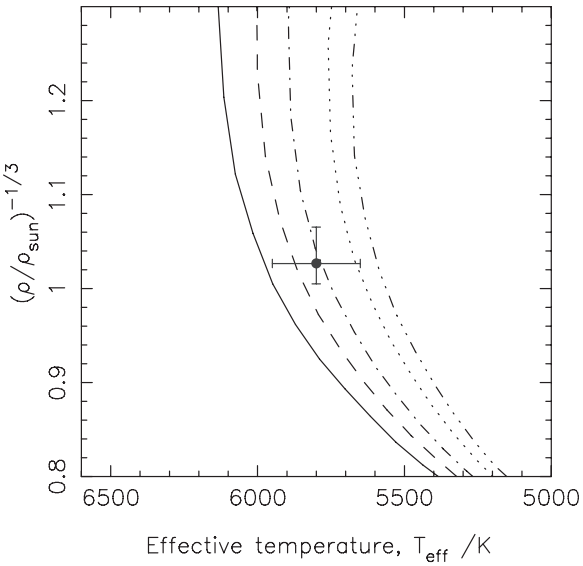

Figure 4. Theoretical stellar isochrones from Yi et al. (2001) plotted as the density proxy $R_*/M_*^{1/3}$ against effective temperature for [Fe/H] = −0.4 and ages 7, 9, 11, 14, and 16 Gyr (from left to right). The position of WASP-37 is indicated within the error ranges.

We find that the measurement of log g from evolutionary models, $\log g_{\rm iso} = 4.39^{+0.02}_{-0.03}$, is consistent with that found from the spectroscopic analysis, $\log g = 4.25 \pm 0.15$. We re-fitted the isochrones using the 1σ upper and lower limits of [Fe/H] and found that this affected the age and mass determinations somewhat, increasing the uncertainties in the age (8–13 Gyr) and stellar mass (0.806–0.914 $M_\odot$).

We computed the stellar distance using the following two methods. First, the absolute bolometric magnitude (calculated from the stellar luminosity) was compared to the extinction-corrected V-band magnitude from TASS ($m_v = 12.7$; Droege et al. 2006). The bolometric correction was taken as the range of values for a G2-type star given in Cox (2000) and Gray (2008). This yielded a distance $D = 338 \pm 41$ pc. Second, we compared the angular diameter $\Theta = 2R_\star/D = 0.025 \pm 0.005$ mas derived from the flux fitting method (see Section 3.1.1) to the stellar radius, yielding a distance $D = 360 \pm 75$ pc. It is reassuring that these values are similar, given that both methods rely on parameters from the stellar models and are therefore not independent. We take the distance to be the weighted mean of the two values, $D = 343 \pm 36$ pc.

3.1.1. Independent Checks

The stellar mass can also be determined through an empirical calibration between $T_{\rm eff}$, $\rho_\star$, and [Fe/H] found from eclipsing binaries (Torres et al. 2010; Enoch et al. 2010). This yields a larger mass, $M_\star = 1.002 \pm 0.034\ M_\odot$, than that from the evolutionary model fit, $M_\star = 0.849^{+0.067}_{-0.040}\ M_\odot$. A possible cause is that WASP-37 is on the edge of the calibration where there are no stars of similar $T_{\rm eff}$, [Fe/H], and log g. A similar situation was found for WASP-21; see Bouchy et al. (2009). In order to obtain a robust result, we have taken the stellar mass to be the average of the two values, $M_\star = 0.925 \pm 0.120\ M_\odot$.

We used archival magnitudes from 2MASS, DENIS, NOMAD, TASS, and CMC14 to derive an independent value of the stellar temperature using the flux-fitting method (Morossi & Malagnini 1985). We find $T_{\rm eff\,flux} = 5840 \pm 140$ K, in excellent agreement with the temperature derived from spectral analysis.

Table 3
Derived Colors of WASP-37

Source	$J-K$	$J-H$	$H-K$
Model	0.377 ± 0.026	0.293 ± 0.026	0.019 ± 0.010
2MASS	0.380 ± 0.032	0.304 ± 0.034	0.076 ± 0.035

Notes. The model colors are derived from stellar evolutionary models and transformed to the 2MASS system. The 2MASS colors are corrected for extinction. See Section 3.1.1 for details.

Independent measures of $v \sin i$ and [Fe/H] can be derived from the shape of the spectral cross correlation function (CCF). Using the empirical calibrations of Boisse et al. (2010) for the SOPHIE HE mode, and inputing Contrast = 4.4% ± 1.3% and FWHM = 9.48 ± 0.06 km s^{-1} from the SOPHIE CCF and $B-V = 0.60 \pm 0.05$ (calculated using Casagrande et al. 2010), we find $[\mathrm{Fe/H}]_{\mathrm{CCF}} = -0.32 \pm 0.17$ and $v \sin i_{\mathrm{CCF}} = 3.2 \pm 1.0$ km s^{-1}. These are also in excellent agreement with the values found from spectral analysis.

The stellar evolution modeling provides color indices which can be compared to observational values. We corrected the 2MASS magnitudes for extinction using $A(V) = 3.1 \times E(B-V)$, appropriately scaled for each passband following Cardelli et al. (1989). The model colors were transformed from the ESO to the 2MASS system following Carpenter (2001). The 2MASS and model colors agree well, as shown in Table 3.

The large relative error on $v \sin i$ provides little constraint on the maximum stellar rotation period $P_{\mathrm{rot}} < 2\pi R_*/v \sin i < 21^{+44}_{-9}$ d, or gyrochronological age: 1–28 Gyr (Barnes 2007). Equally, the lithium abundance only implies a lower limit on the age of 1–2 Gyr (Sestito & Randich 2005).

Given the low metallicity of WASP-37, we investigated whether it could be a member of the thick disk using the method outlined in Bouchy et al. (2010). We calculated the space velocities according to Johnson & Soderblom (1987), using the proper motions, distance, and γ given in Tables 2 and 4. The velocities were updated to J2000 and corrected for solar motion using data from Dehnen & Binney (1998) giving $U = -27.2 \pm 3.4$ km s^{-1}, $V = 7.8 \pm 14.0$ km s^{-1}, and $W = 45.5 \pm 4.4$ km s^{-1} (right-hand coordinate system).

In order to quantify the probability that WASP-37 is a member of the thick disk, we compared its metallicity and space velocities to the properties of similar stars in the Besançon Galactic model (Robin et al. 2003). We generated 78,000 model stars in 20 realizations and returned all stars with apparent magnitudes between $m_{\mathrm{v}} = 8$ and 16, spectral type F5–K9 and luminosity class IV and V for 30 deg^2 in the direction of WASP-37 (galactic coordinates $l = 356°$, $b = 53°$, NED). For the stars with [Fe/H] and space velocities within 3σ of WASP-37, half were members of the old thin disk (>6 Gyr), one-third were part of the thick disk, and the remainder were 1.5–6 Gyr thin disk members. Abundance analysis shows that WASP-37 has enhanced alpha elements and although this is not accounted for in the simulation, we estimate that it increases the probability of thick disk membership but that it is also equally likely to be part of the old thin disk. It is reassuring that this independent analysis also finds that WASP-37 is part of an old population.

3.2. Planet Parameters

To determine the properties of the planet, we simultaneously modeled the SuperWASP, LT, and FTN light curves and the CORALIE and SOPHIE RVs with a global MCMC fit. Details of this process are described in Cameron et al. (2007) and Pollacco et al. (2008). The free parameters in the fit are orbital period P, transit epoch T_0, transit duration T_{dur}, ratio of planet to star radius $(R_{\mathrm{p}}/R_*)^2$, impact parameter b, RV semi-amplitude K, Lagrangian elements $e \cos \omega$ and $e \sin \omega$ where e is the eccentricity and ω is the longitude of periastron, and the systematic offset velocity γ. In this particular case, two systematic velocities were fitted to allow for instrumental offsets between the SOPHIE and CORALIE data sets.

Table 4
System Parameters of WASP-37b

Parameter (Unit)	Value
Photometric parameters	
P (d)	3.577469 ± 0.000011
T_0 (HJD)	2455338.6188 ± 0.0006
T_{dur} (d)	$0.1304^{+0.0018}_{-0.0017}$
$\Delta F = (R_{\mathrm{P}}/R_*)^2$	$0.01427^{+0.00030}_{-0.00023}$
R_{P}/R_*	$0.11946^{+0.00126}_{-0.00096}$
a/R_*	9.567 ± 0.648
b	$0.198^{+0.132}_{-0.128}$
i(°)	$88.82^{+0.77}_{-0.86}$
Spectroscopic parameters	
K (km s^{-1})	0.2507 ± 0.0084
γ_{SOPHIE} (km s^{-1})	7.9714 ± 0.0024
$\gamma_{\mathrm{CORALIE}}$ (km s^{-1})	7.9116 ± 0.0024
e	0 (fixed)
Derived parameters	
M_{p} (M_{J})	1.80 ± 0.17
R_{p} (R_{J})	$1.16^{+0.07}_{-0.06}$
$\rho_{\mathrm{P}}(\rho_{\mathrm{J}})$	$1.15^{+0.12}_{-0.15}$
log g_{P} (cgs)	$3.48^{+0.03}_{-0.04}$
a (AU)	0.0446 ± 0.0019
$T_{\mathrm{eq},A=0}$ (K)	1323^{+25}_{-15}

Table 5
Limb Darkening Coefficients

Light Curve	Band	a_1	a_2	a_3	a_4
SuperWASP	R	0.643	−0.278	0.800	−0.413
RISE	V	0.570	−0.131	0.791	−0.420
FTN	Z	0.623	−0.331	0.672	−0.346

We propagated the uncertainty in the stellar mass through to the derived parameters ($M_\star = 0.925 \pm 0.120\,M_\odot$; see Section 3.1.1). We used the four Claret (2000, 2004) nonlinear limb darkening coefficients for the appropriate stellar temperature and photometric passband appropriate for each light curve; see Table 5. The limb darkening coefficients are re-calculated at each step in the MCMC chain to take into account the uncertainties in the stellar temperature and radius.

The photometric error bars were scaled to account for any underestimations so that the best-fitting model results in $\chi^2_{\mathrm{red}} = \chi^2/\mathrm{dof} = 1$ (dof = number of points − number of fitted parameters). The RV error bars did not require rescaling with a jitter term in order to obtain $\chi^2_{\mathrm{red}} = 1$. The rms of the residuals from the best-fit model are $\mathrm{rms}_{\mathrm{WASP}} = 0.0292$ mag, $\mathrm{rms}_{\mathrm{LT}} = 0.0013$ mag, $\mathrm{rms}_{\mathrm{FTS}} = 0.0025$ mag, $\mathrm{rms}_{\mathrm{SOPHIE}} = 0.0194$ km s^{-1}, and $\mathrm{rms}_{\mathrm{CORALIE}} = 0.0380$ km s^{-1}. By removing the outlying point at 8.064 km s^{-1}, we obtain $\mathrm{rms}_{\mathrm{CORALIE}} = 0.0164$ km s^{-1}.

An initial fit was performed in which the eccentricity was allowed to float, yielding $e = 0.036 \pm 0.021$. From the Lucy–Sweeney test (Lucy & Sweeney 1971), we find it is only

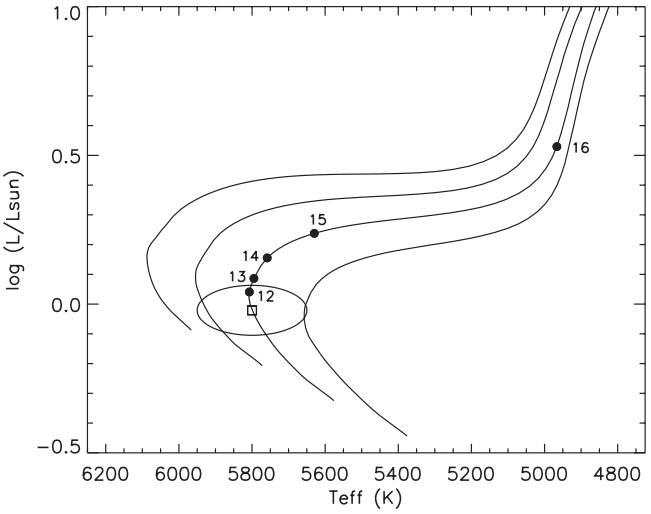

Figure 5. Evolutionary mass tracks from Yi et al. (2001) for [Fe/H] = −0.4 and stellar masses of 0.95, 0.9, 0.85, and 0.8 $M_{\odot}$ (from left to right). The current position of WASP-37 is shown as a square within the 1σ uncertainty ellipse. The 12, 13, 14, 15, and 16 Gyr points are shown on the best-fit, 0.85 $M_{\odot}$ track. WASP-37 is predicted to evolve onto the subgiant branch at age ∼15 Gyr and red giant branch ∼1 Gyr later.

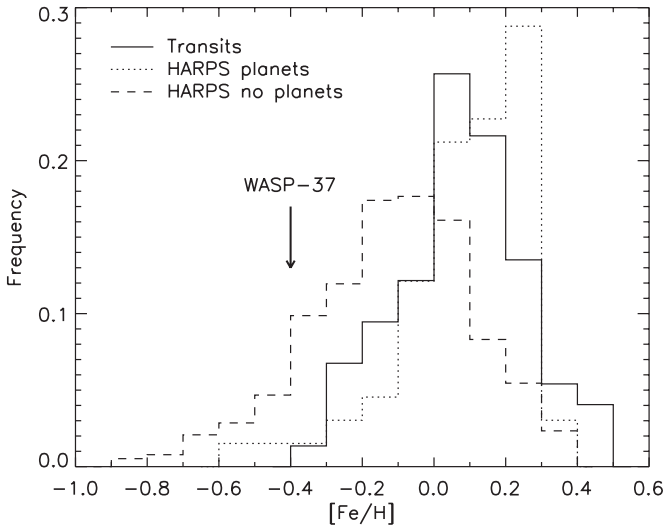

Figure 6. Histogram of the metallicity of transiting planet host stars and stars with and without detections of RV planets from the HARPS GTO "high-precision" sample (Sousa et al. 2008). WASP-37 is clearly in the tail of the metallicity distribution for stars hosting planets.

significant at the 1σ level, and hence a circular orbit was adopted ($\chi^2_{\rm circ} = 18.3$, $\chi^2_{\rm ecc} = 14.0$ with 13 RVs and 5 free parameters: K, $\gamma_{\rm CORALIE}$, $\gamma_{\rm SOPHIE}$, $e\cos\omega$, and $e\sin\omega$). We determined an upper limit for the eccentricity as $e_{\rm upper} = e + 3\sigma = 0.078$. We also fitted a linear trend in the RVs to search for a third body in the system, but found that the decrease in χ^2 did not warrant the extra free parameter. From the F-test, we found that the significance of the trend was less than 1σ ($\chi^2 = 18.3$, $\chi^2_{\rm trend} = 15.4$ with 13 RVs and 4 free parameters: K, $\gamma_{\rm CORALIE}$, $\gamma_{\rm SOPHIE}$, and linear trend $\dot{\gamma}$).

We performed the final MCMC fit with a chain length of 20,000 points and the resulting best-fit parameters and uncertainties are shown in Table 4. WASP-37b has $P = 3.577469 \pm 0.000011$ d, $M_{\rm p} = 1.80 \pm 0.17\ M_{\rm J}$, $R_{\rm p} = 1.16^{+0.07}_{-0.06}\ R_{\rm J}$, and $\rho_{\rm p} = 1.15^{+0.12}_{-0.15}\ \rho_{\rm J}$.

4. DISCUSSION

We report the discovery of a new transiting hot Jupiter, WASP-37b. The planet has a radius comparable to Jupiter ($R_{\rm p} = 1.16^{+0.07}_{-0.06}\ R_{\rm J}$) but is more massive ($M_{\rm p} = 1.80 \pm 0.17\ M_{\rm J}$) and hence is very similar to WASP-5 (Anderson et al. 2008; Southworth et al. 2009). The surface gravity of WASP-37b is high compared to other planets with similar orbital periods ($\log g_{\rm p} = 3.48^{+0.03}_{-0.04}$, $g_{\rm p} = 30.2^{+2.0}_{-2.8}$ ms^{-2}, $\rho_{\rm p} = 1.15^{+0.12}_{-0.15}\ \rho_{\rm J}$), which lies significantly above the period–gravity correlation proposed by Southworth (2010).

By comparison with the theoretical models of Fortney et al. (2007) and Baraffe et al. (2008), we find that WASP-37b has an inflated radius. The models do not cover the age range of WASP-37; however given that planetary radii are thought to decrease with age, the expected radius of WASP-37b will be smaller than those given for the oldest model. For an equivalent semi-major axis with solar insolation of 0.445 AU, the measured mass and radius do not suggest the presence of a core of heavy elements for models older than 1 Gyr, and this is consistent with the correlation between core mass and metallicity (Guillot et al. 2006; Burrows et al. 2007) given the low stellar metallicity.

We detect no significant orbital eccentricity and find an upper limit of 0.098. Nor do we find evidence of any long-term trend caused by a third body. Our RV observations span ∼70 days and continued monitoring would reveal the presence of any longer-term trends and further constrain the eccentricity.

With a stellar effective temperature of 5800 ± 150 K and orbital period of 3.577469 ± 0.000011 d, the planet is predicted to have an equilibrium temperature of 1323^{+25}_{-15} K (assuming zero albedo and full redistribution of the incident radiation). Secondary eclipse measurements of WASP-37 may be a way of constraining the influence of metallicity on the presence or not of atmospheric temperature inversions.

The relatively large uncertainties in the stellar parameters are caused by the low S/N of the combined spectrum used for spectral analysis, due to the faintness of the target ($m_{\rm v} = 12.7$). Further spectra would help to constrain the spectroscopic and derived parameters. A more precise value of $v\sin i$ could also be found from an observation of the Rossiter–McLaughlin (RM) effect (Rossiter 1924; McLaughlin 1924; Gaudi & Winn 2007), which could provide an independent constraint on the age through gyrochronological relations (Barnes 2007). The slow rotation ($v\sin i = 2.4 \pm 1.6$ km s^{-1}) and faintness of the host star would make observations of the RM effect challenging but possible given the predicted amplitude of 35 m s^{-1}.

We find a small discrepancy between the stellar mass found from evolutionary models and empirical calibrations based on eclipsing binaries, and take a mean of the two values in this analysis. WASP-37 is less massive than the Sun, $M_{\star} = 0.925 \pm 0.120\ M_{\odot}$, and at ∼11 Gyr is one of the older stars hosting a transiting planet. Although the age is relatively uncertain, it suggests that giant planet formation was taking place when the Milky Way was still relatively young. The model isochrone, shown in Figure 5, suggests that WASP-37 is due to evolve from a main-sequence star into a subgiant at an age of ∼15 Gyr and subsequently move on to the giant branch after a further ∼1 Gyr. Although no meaningful constraint can be placed on the stellar tidal quality factor, Q_s, we note that if is greater than 10^7 then the planetary spiral-in timescale (Levrard et al. 2009) is longer than the main-sequence lifetime, and the planet will be engulfed by the expansion of the stellar radius during the giant phase less than 0.5 Gyr after the star has evolved onto the giant branch.

WASP-37 has the second lowest metallicity ([Fe/H] = -0.4 ± 0.12) of the transiting planet host stars after WASP-21 (Bouchy et al. 2010), and is firmly in the tail of the metallicity distribution for exoplanet host stars as shown in Figure 6. The figure, similar to that in Ammler-von Eiff et al. (2009), shows the metallicity distributions for stars with transiting planets and stars with and without detections of RV planets from the HARPS GTO "high-precision" sample (Sousa et al. 2008). The stars hosting transiting and RV planets show a very similar distribution, whereas the non-planet hosts appear to extend to much lower metallicities, suggesting that the heavy metal content plays a significant role in planet formation (Gonzalez 1998; Santos et al. 2004; Fischer & Valenti 2005).

The SuperWASP Consortium consists of astronomers primarily from Queen's University Belfast, St Andrews, Keele, Leicester, The Open University, Isaac Newton Group La Palma, and Instituto de Astrofõsica de Canarias. The SuperWASP-N camera is hosted by the Isaac Newton Group on La Palma and WASP-South is hosted by SAAO. We are grateful for their support and assistance. Funding for WASP comes from consortium universities and from the UK's Science and Technology Facilities Council. F.P.K. is grateful to AWE Aldermaston for the award of a William Penny Fellowship. Based on observations made at Observatoire de Haute Provence (CNRS), France and at the ESO La Silla Observatory (Chile) with the CORALIE Echelle spectrograph mounted on the Swiss telescope. The RISE instrument mounted in the Liverpool Telescope was designed and built with resources made available from Queen's University Belfast, Liverpool John Moores University, and the University of Manchester. The Liverpool Telescope is operated on the island of La Palma by Liverpool John Moores University in the Spanish Observatorio del Roque de los Muchachos of the Instituto de Astrofisica de Canarias with financial support from the UK Science and Technology Facilities Council. The research leading to these results has received funding from the European Community's Seventh Framework Programme (FP7/2007-2013) under grant agreement number RG226604 (OPTICON). We thank Tom Marsh for the use of the ULTRACAM pipeline.

REFERENCES

Ammler-von Eiff, M., et al. 2009, A&A, 507, 523
Anderson, D. R., et al. 2008, MNRAS, 387, L4
Anderson, D. R., et al. 2010, ApJ, 709, 159
Baraffe, I., Chabrier, G., & Barman, T. 2008, A&A, 482, 315
Baranne, A., et al. 1996, A&ASS, 119, 373
Barnes, S. A. 2007, ApJ, 669, 1167
Barros, S. C. C. 2010, A&A, submitted (arXiv:1010.0849)
Boisse, I., et al. 2010, A&A, 523, A88
Bouchy, F., et al. 2009, A&A, 505, 853
Bouchy, F., et al. 2010, A&A, 519, A98
Burrows, A., Hubeny, I., Budaj, J., & Hubbard, W. B. 2007, ApJ, 661, 502
Cameron, A. C., et al. 2006, MNRAS, 373, 799
Cameron, A. C., et al. 2007, MNRAS, 375, 951
Cardelli, J. A., Clayton, G. C., & Mathis, J. S. 1989, ApJ, 345, 245
Carpenter, J. M. 2001, AJ, 121, 2851
Casagrande, L., Ramírez, I., Meléndez, J., Bessell, M., & Asplund, M. 2010, A&A, 512, A54
Claret, A. 2000, A&A, 363, 1081
Claret, A. 2004, A&A, 428, 1001
Cox, A. N. 2000, Allen's Astrophysical Quantities (New York: AIP), 388
Dehnen, W., & Binney, J. J. 1998, MNRAS, 298, 387
Dhillon, V. S., et al. 2007, MNRAS, 378, 825
Droege, T. F., Richmond, M. W., Sallman, M. P., & Creager, R. P. 2006, PASP, 118, 1666
Enoch, B., Cameron, A. C., Parley, N. R., & Hebb, L. 2010, A&A, 516, A33
Fischer, D. A., & Valenti, J. 2005, ApJ, 622, 1102
Fortney, J. J., Marley, M. S., & Barnes, J. W. 2007, ApJ, 659, 1661
Fossey, S. J., Waldmann, I. P., & Kipping, D. M. 2009, MNRAS, 396, L16
Garcia-Melendo, E., & McCullough, P. R. 2009, ApJ, 698, 558
Gaudi, B. S., & Winn, J. N. 2007, ApJ, 655, 550
Gibson, N. P., et al. 2008, A&A, 492, 603
Gillon, M., et al. 2009, A&A, 496, 259
Gonzalez, G. 1998, A&A, 334, 221
Gray, D. F. 2008, The Observation and Analysis of Stellar Photospheres (Cambridge: Cambridge Univ. Press)
Guillot, T., et al. 2006, A&A, 453, L21
Haswell, C. A. 2010, Transiting Exoplanets (Cambridge: Cambridge Univ. Press)
Hebb, L., et al. 2010, ApJ, 708, 224
Johnson, D. R. H., & Soderblom, D. R. 1987, AJ, 93, 864
Latham, D. W., et al. 2010, ApJ, 713, L140
Laughlin, G., et al. 2009, Nature, 457, 562
Levrard, B., Winisdoerffer, C., & Chabrier, G. 2009, ApJ, 692, L9
Lucy, L. B., & Sweeney, M. A. 1971, AJ, 76, 544
Magain, P. 1984, A&A, 134, 189
McLaughlin, D. B. 1924, ApJ, 60, 22
Morossi, C., & Malagnini, M. L. 1985, A&AS, 60, 365
Moutou, C., Hébrard, G., Bouchy, F., Eggenberger, A., & Boisse, I. 2009, A&A, 498, L5
Munari, U., & Zwitter, T. 1997, A&A, 318, 269
Naef, D., et al. 2001, A&A, 375, L27
Pepe, F., et al. 2002, A&A, 388, 632
Perruchot, S., Kohler, D., Bouchy, F., Richaud, Y., & Richaud, P. E. 2008, Proc. SPIE, 7014, 17
Pollacco, D. L., et al. 2006, PASP, 118, 1407
Pollacco, D., et al. 2008, MNRAS, 385, 1576
Queloz, D., et al. 2001, A&A, 379, 279
Robin, A. C., Reylé, C., Derrière, S., & Picaud, S. 2003, A&A, 409, 523
Rossiter, R. A. 1924, ApJ, 60, 15
Santos, N. C., Israelian, G., & Mayor, M. 2004, A&A, 415, 1153
Sestito, P., & Randich, S. 2005, A&A, 442, 615
Skrutskie, M. F., et al. 2006, AJ, 131, 1163
Sousa, S. G., et al. 2008, A&A, 487, 373
Southworth, J. 2010, MNRAS, 408, 1689
Southworth, J., et al. 2009, MNRAS, 396, 1023
Sozzetti, A., et al. 2007, ApJ, 664, 1190
Steele, I. A., et al. 2008, Proc. SPIE, 7014, 217
Toner, C. G., & Gray, D. F. 1988, ApJ, 334, 1008
Torres, G., Andersen, J., & Giménez, A. 2010, A&AR, 18, 67
Yi, S., et al. 2001, ApJS, 136, 417
Zacharias, N., et al. 2005, VizieR Online Data Catalog, 1297, 0